On the acoustic analysis and optimization of ducted ventilation systems using a sub-structuring approach

X. Yu,[1] F. S. Cui,[1] and L. Cheng[2,a)]
[1]*Institute of High Performance Computing, Agency for Science, Technology and Research, Singapore, Singapore*
[2]*Department of Mechanical Engineering, The Hong Kong Polytechnic University, Hong Kong, China*

(Received 18 November 2015; revised 16 December 2015; accepted 28 December 2015; published online 13 January 2016)

This paper presents a general sub-structuring approach to predict the acoustic performance of ducted ventilation systems. The modeling principle is to determine the subsystem characteristics by calculating the transfer functions at their coupling interfaces, and the assembly is enabled by using a patch-based interface matching technique. For a particular example of a bended ventilation duct connecting an inlet and an outlet acoustic domain, a numerical model is developed to predict its sound attenuation performance. The prediction accuracy is thoroughly validated against finite element models. Through numerical examples, the rigid-walled duct is shown to provide relatively weak transmission loss (TL) across the frequency range of interest, and exhibit only the reactive behavior for sound reflection. By integrating sound absorbing treatment such as micro-perforated absorbers into the system, the TL can be significantly improved, and the system is seen to exhibit hybrid mechanisms for sound attenuation. The dissipative effect dominates at frequencies where the absorber is designed to be effective, and the reactive effect provides compensations at the absorption valleys attributed to the resonant behavior of the absorber. This ultimately maintains the system TL at a relatively high level across the entire frequency of interest. The TL of the system can be tuned or optimized in a very efficient way using the proposed approach due to its modular nature. It is shown that a balance of the hybrid mechanism is important to achieve an overall broadband attenuation performance in the design frequency range.
© *2016 Acoustical Society of America*. [http://dx.doi.org/10.1121/1.4939785]

[NX] Pages: 279–289

I. INTRODUCTION

Natural ventilation in buildings is an attractive topic for living comfort improvement and sustainable development. The airflow and thermal performances as the primary factors have been extensively studied.[1] However, ventilation apertures by opening large areas of building façades offer little resistance to noise passage. This could limit the potential of using natural ventilation in high noise concentration areas such as the major metropolitan cities. Typically, for an acoustically hard-walled building facade containing an aperture, its sound reduction index tends to be dominated by the aperture, even though its area is much smaller than that of the wall.[2]

There always seems to be a conflict between natural ventilation and acoustic insulation. Among possible acoustic treatments reported in the literature, the sound barrier[2] and acoustic louver[3] are effective in screening the direct sound incidence in relatively high frequency range, but they cannot handle low frequency noise due to the long wavelength character of sound. The quarter wave or Helmholtz resonators[4] can be specially designed for suppressing the low frequency noise within a narrow frequency band, but the attenuation provided for an aperture is usually weak due to the limited space available.

The strategy of using a ducted ventilation system may provide possibilities to reduce the noise ingress while maintaining sufficient airflow passage. In general, the noise control treatment has more opportunity to be applied inside the ductwork compared with the limited space surrounding an aperture. For example, De Salis *et al.*[5] reviewed a number of noise control techniques for naturally ventilated buildings, and suggested that a ventilation duct could embrace the use of absorbing treatments as well as active noise cancellation. Kang and Brocklesby[6] proposed a ventilation window design by staggering two layers of glass panels, between which transparent micro-perforated absorbers were added to reduce the sound transmission. Numerical simulations were later conducted by varying window design parameters,[7] and Huang *et al.*[8] further applied an active noise control technique to suppress the low frequency noise penetrating through the window system. Moreover, Wang *et al.*[9] compared the effectiveness of using quarter wave resonators or membrane absorbers in a ducted ventilation window. Concurrent use of both active noise and vibration control in a ventilation duct was also examined by Rohlfing and Gardonio.[10]

Whilst the potential of using a ducted ventilation system for noise control is promising, research into the numerical analysis and optimization of its acoustic performance has been fairly limited, possibly due to the numerous challenges faced by the conventional modeling approaches. For example, analytical approaches based on the modal description of

a)Electronic mail: li.cheng@polyu.edu.hk

acoustic waves can only handle simple system geometries. The Finite Element Method (FEM) provides a powerful tool in solving coupled physical problems, but the number of discretized nodes and induced computational cost drastically increase as the system dimension is large or the targeted frequencies are high. This becomes even more crucial when parametric studies or system optimizations are needed. In contrast to the deterministic models, Statistical Energy Analysis offers a rough analysis tool at high frequency range.[11] But it may not be applicable here since the noise ingress into the building mainly concentrates in the low-to-mid frequency range. Also, the results predicted from a statistical approach are too rough to enable a clear understanding of the sound transmission mechanisms.

In tackling these challenges, this paper presents a general sub-structuring approach for the acoustic analysis and optimization of ducted ventilation systems. The basic principle is to decouple the complex system into a number of subsystems which can be modeled separately, and the overall system response is solved by using a transfer function based assembling treatment. For a convenient interface description, the connecting surface between two subsystems is meshed into a set of patch elements. It is assumed that the distributed points within a patch exhibit a similar vibrational response under excitation, so that an averaged property is enough to characterize the behavior of each patch. The validity of this assumption can be ensured by the patch division criteria compared with the minimum acoustic wavelength of interest.[12] In this way, the patch based interface matching requires less number of degrees of freedom (n-DOF) compared with the traditional point collocation technique,[13] and the required computational cost is drastically reduced. Meanwhile, the determination of the subsystem properties using the proposed approach can be performed by using an open selection of numerical or even experimental tools.[12] This provides a more flexible option for subsystem description compared with the analytical mode matching technique.[14]

In this paper, the modeling framework of the proposed sub-structuring approach is first established by considering a generic ducted ventilation system in Sec. II, where the general structural-acoustic coupling using the patch based interface matching is formulated. A numerical model is further developed for the prediction of its sound attenuation performance. Given a particular system configuration in Sec. III, the prediction accuracy using the proposed approach is validated against FEM simulations, and the associated computational costs are compared. Then, non-fibrous micro-perforated panel (MPP) absorbers are used inside the ventilation duct to increase its sound attenuation performance. The study not only demonstrates the effectiveness of MPP through sound absorption enhancement, but also reveals the underlying sound attenuation mechanisms. Based on a brief parametric study, the sensitivity of the system response to parameter variations is discussed, suggesting that a tunable acoustic performance can be achieved in a targeted frequency range. Subsequently, two optimization case studies are presented by tuning the associated parameters, which demonstrates the capability and the computation efficiency of the proposed approach.

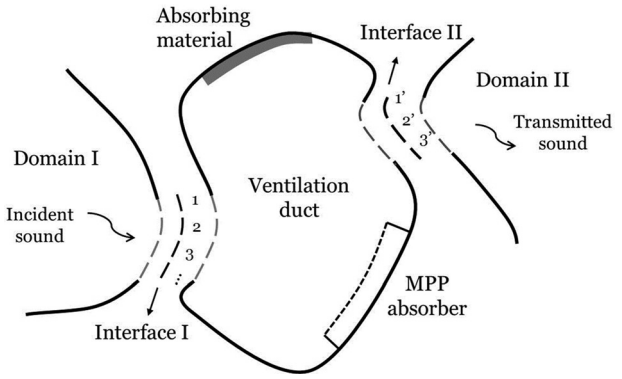

FIG. 1. An example of a ducted ventilation system being inserted into a building facade.

II. FORMULATION

Consider a generic example representing a ducted ventilation system being inserted into a building facade as shown in Fig. 1. From the acoustic viewpoint, the ventilation duct is simply an acoustic waveguide connecting the exterior and interior acoustic media. The ductwork incorporates spatial distortions such as bends to avoid significant length, which also helps screen the direct path for noise ingress. Without loss of generality, the ventilation duct in Fig. 1 can be either rigid-walled or integrated with noise control treatments such as porous absorbent material and non-fibrous MPP absorbers. The incident sound waves reaching the inlet aperture can be due to any sound sources such as road traffic, and the transmitted sound waves from the outlet aperture describe the noise leakage into the building interior.

The entire system is divided into three acoustic subsystems and two coupling interfaces, I and II, as shown in Fig. 1. Each interface may be defined implicitly as a vibrating boundary surface like a flexible panel. For convenience in the coupling treatment, each interface is segmented into a set of patches, acting as the coupling agents or energy channels between subsystems. The two interfaces, I and II, in Fig. 1 are meshed into N and N′ patches, respectively. For deterministic analysis, the patch size needs to be properly selected, small enough to describe the short-wavelength behavior of the waves. An appropriate patch division criteria of $\Delta_{\text{patch}} < \lambda_s/2$ has been suggested and discussed by Ouisse *et al.* in a previous publication,[12] where Δ_{patch} is the required patch size and λ_s is the minimum acoustic wavelength of interest.

For a general separation interface with N patches segmented over its surface, the relationship between the excitation force and velocity response can be written as

$$\mathbf{U} = \mathbf{Y} \cdot \mathbf{F} = \begin{bmatrix} Y_{11} & Y_{12} & \cdots \\ Y_{21} & \ddots & \\ \vdots & & Y_{NN} \end{bmatrix} \cdot \begin{bmatrix} F_1 \\ \vdots \\ F_N \end{bmatrix} = \begin{bmatrix} U_1 \\ \vdots \\ U_N \end{bmatrix}, \tag{1}$$

where **Y** is the mobility matrix of the interface, a square matrix of order N; **F** is the column vector of the excitation force applied to each patch, both the mechanical and acoustical

excitations are combined; and $\mathbf{U}$ is the column vector of the averaged patch velocity, as the steady-state response of the interface.

If the separation boundary presents itself in a fully coupled vibroacoustic environment, its vibration will also cause disturbance to the connected acoustic domains. The acoustic loading on either side of the interface due to such coupling can be expressed as

$$\mathbf{F}_{\mathrm{a}} = \mathbf{Z}_{\mathrm{a}} \cdot \mathbf{U}, \tag{2}$$

where $\mathbf{Z}_{\mathrm{a}}$ is the impedance matrix of the acoustic domain and $\mathbf{F}_{\mathrm{a}}$ is the acoustic loading force resulted from the vibration of the interface.

Then, based on the linear superposition principle, the generalized structural-acoustic coupling formulation for an interface can be described as

$$\mathbf{Y} \cdot (\mathbf{F}_{\mathrm{ext}} + \mathbf{Z}_l \cdot \mathbf{U} + \mathbf{Z}_r \cdot \mathbf{U}) = \mathbf{U}, \tag{3}$$

where $\mathbf{Z}_l$ and $\mathbf{Z}_r$ are the impedances of the coupled acoustic domain, e.g., on the left- and right-hand side of the interface. $\mathbf{F}_{\mathrm{ext}}$ describes any external excitation force applied to the interface.

In special cases when the interface is better characterized as an impedance surface, Eq. (3) changes to

$$\mathbf{F}_{\mathrm{ext}} + \mathbf{Z}_l \cdot \mathbf{U} + \mathbf{Z}_r \cdot \mathbf{U} = \mathbf{Z} \cdot \mathbf{U}, \tag{4}$$

where $\mathbf{Z}$ is the impedance matrix of the surface. It should be noted that the mobility and impedance matrices in Eqs. (3) and (4), for both the interface and connected acoustic domains, are independent of external excitation force $\mathbf{F}_{\mathrm{ext}}$ and thus considered as the inherent properties of the subsystems. These properties are determined individually before the assembly.

Consider now the coupling between the two interfaces through the ventilation duct in Fig. 1. The coupled equations can be derived by extending the generalized Eq. (3) to incorporate a mutual coupling term as

$$\begin{aligned} \mathbf{Y}^{\mathrm{I}}(\mathbf{F}^{\mathrm{I}}_{\mathrm{ext}} + \mathbf{Z}^{\mathrm{I}}_l\mathbf{U}^{\mathrm{I}} + \mathbf{Z}^{\mathrm{I}}_r\mathbf{U}^{\mathrm{I}} + \mathbf{Z}^{\mathrm{I-II}}\mathbf{U}^{\mathrm{II}}) &= \mathbf{U}^{\mathrm{I}}, \\ \mathbf{Y}^{\mathrm{II}}(\mathbf{F}^{\mathrm{II}}_{\mathrm{ext}} + \mathbf{Z}^{\mathrm{II}}_l\mathbf{U}^{\mathrm{II}} + \mathbf{Z}^{\mathrm{II}}_r\mathbf{U}^{\mathrm{II}} + \mathbf{Z}^{\mathrm{II-I}}\mathbf{U}^{\mathrm{I}}) &= \mathbf{U}^{\mathrm{II}}, \end{aligned} \tag{5}$$

where $\mathbf{F}^{\mathrm{I}}_{\mathrm{ext}}$ and $\mathbf{F}^{\mathrm{II}}_{\mathrm{ext}}$ are the external force vectors applied to the two interfaces. $\mathbf{Z}^{\mathrm{I}}_l$ and $\mathbf{Z}^{\mathrm{I}}_r$ are the impedance matrices describing the acoustic domains on both sides of interface I (the same applies to interface II). $\mathbf{Z}^{\mathrm{I-II}}$ is the coupling impedance between the two interfaces, used for describing the acoustic loading force exerted on interface I due to a vibrating interface II. Note that the matrix size of $\mathbf{Z}^{\mathrm{I-II}}$ is $\mathrm{N} \times \mathrm{N}'$, and $\mathbf{Z}^{\mathrm{II-I}} = (\mathbf{Z}^{\mathrm{I-II}})^{\mathrm{T}}$ according to the acoustic reciprocity theory (T stands for transpose operation).

Then, the coupled equations governing the overall system response can be summarized into the following form:

$$\begin{bmatrix} \mathbf{T}^{\mathrm{I}}_l & \mathbf{T}_c \\ \mathbf{T}_c{}^{\mathrm{T}} & \mathbf{T}^{\mathrm{II}}_l \end{bmatrix} \begin{bmatrix} \mathbf{U}^{\mathrm{I}} \\ \mathbf{U}^{\mathrm{II}} \end{bmatrix} = \begin{bmatrix} \mathbf{F}^{\mathrm{I}}_{\mathrm{ext}} \\ \mathbf{F}^{\mathrm{II}}_{\mathrm{ext}} \end{bmatrix}, \tag{6}$$

where

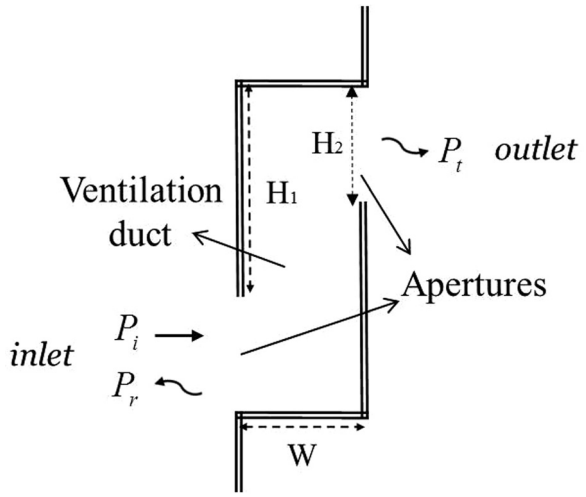

FIG. 2. A representative ventilation duct with rigid internal surfaces and right-angled bends.

$$\begin{aligned} \mathbf{T}^{\mathrm{I}}_l &= (\mathbf{Y}^{\mathrm{I}})^{-1} - (\mathbf{Z}^{\mathrm{I}}_l + \mathbf{Z}^{\mathrm{I}}_r), \\ \mathbf{T}^{\mathrm{II}}_l &= (\mathbf{Y}^{\mathrm{II}})^{-1} - (\mathbf{Z}^{\mathrm{II}}_l + \mathbf{Z}^{\mathrm{II}}_r), \\ \mathbf{T}_c &= -\mathbf{Z}^{\mathrm{I-II}}. \end{aligned} \tag{7}$$

It can be seen that the transfer functions T_l depend on the mobility and impedance at the interface locally, whereas the transfer function T_c describes the mutual interactions between the two interfaces. Up to this point, the solution procedure using the proposed sub-structuring approach can be briefly summarized as follows:

(1) The system ensemble is decoupled into a set of subsystems by their separation interfaces.
(2) A sufficient number of patches are defined for each interface. Then, the local mobility for the interface, the impedances for the acoustic subsystems are determined (detailed formulations will be demonstrated later).
(3) The general structural-acoustic coupling formulation in Eq. (3) is employed to perform the system assembling treatment, and the coupled system response is solved.

The proposed sub-structuring approach provides a systematic numerical framework rather than a particular technique to describe the complex vibroacoustic interactions between subsystems. The subsystem properties can be determined by employing a broad selection of well-developed numerical methods such as modal approach, FEM, or even a direct experiment, as long as the transfer function information defined at each interface can be obtained. This enables hybrid models[15] (e.g., hybrid modal-FEM[16]) to be built, if the subsystems have significantly different orders of n-DOF. Furthermore, with an aim to conduct system optimization, the proposed approach can greatly reduce the computational cost benefiting from the modular treatment.

Then, consider a specific example of a ventilation duct as shown in Fig. 2. The duct is first assumed to have rigid internal surfaces and right-angled bends, whose total height is defined as $\mathrm{H}_1 + \mathrm{H}_2$ in Fig. 2, with H_2 being the aperture size. It is noted that although a two-dimensional example is

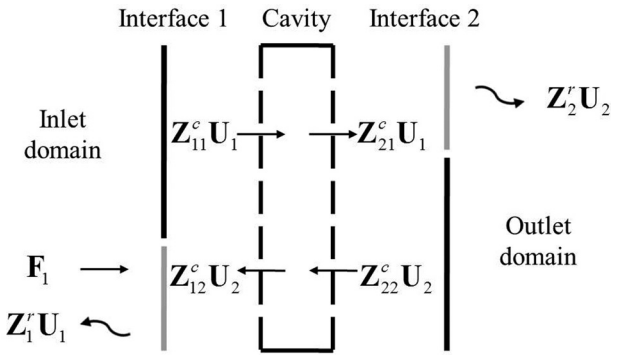

FIG. 3. Vibroacoustic modeling of the system shown in Fig. 2 using the proposed sub-structuring approach.

presented here in the figure, the following formulation is generally applicable to three-dimensional cases without any technical hurdles.

At the duct inlet, the sound field corresponding to the exterior of the building facade can be described as

$$P_{\text{in}} = P_i + P_r, \tag{8}$$

where P_i and P_r are the incident and reflected sound waves, respectively. Typically, P_i can be either due to specific sound sources such as road traffic, or simply assumed as plane wave incidence for general analysis.

The leakage noise from the outlet domain into the building interior is

$$P_{\text{out}} = P_t, \tag{9}$$

where P_t is the transmitted sound waves, radiated from the outlet opening.

Using the sub-structuring approach, the system is partitioned into three acoustic subsystems and two interfaces, as shown in Fig. 3. The two interfaces, 1 and 2, consist of an aperture and a rigid or flexible structure, which are systematically modeled using a proposed Compound Interface treatment[17] by writing their mobilities as

$$\mathbf{Y}_1 = \begin{bmatrix} \mathbf{Y}_s & \\ & \mathbf{Y}_o \end{bmatrix}; \quad \mathbf{Y}_2 = \begin{bmatrix} \mathbf{Y}_o & \\ & \mathbf{Y}_s \end{bmatrix}, \tag{10}$$

where Y_o is the equivalent mobility of the aperture by formulating it as a virtual panel;[18] Y_s is the structural mobility of the rigid or flexible structure. The detailed formulations for the aperture and structure have been well-established in Ref. 18 and are not repeated here.

The rigid ventilation duct with right-angled bends can be well represented by viewing it as an acoustic cavity. For illustration purposes, the formulation procedure for determining its acoustic impedances by using a modal decomposition approach is presented here. Without loss of generality, the sound pressure field in a three-dimensional acoustic cavity can be expanded into the modal coordinates as

$$p_c(x,y,z) = \sum_m a_c^m \varphi_c^m, \tag{11}$$

where p_c is the sound pressure at any point inside the cavity; a_c^m is the mth modal amplitude of the cavity; φ_c^m is the mode shape function.

For a cavity consisting of a domain V_c and a boundary S_c, the pressure field inside the cavity can be described through Green's function[19,20]

$$\int_{V_c} \left(p_c \nabla^2 \varphi_c^m - \varphi_c^m \nabla^2 p_c\right) dV_c = \int_{s_c} \left(p_c \frac{\partial \varphi_c^m}{\partial n} - \varphi_c^m \frac{\partial p_c}{\partial n}\right) dS_c. \tag{12}$$

On inserting the Helmholtz equation which governs the sound wave propagation and making use of the modal orthogonality further gives

$$a_c^m N_c^m \left(k^2 - k_m^2\right) = \int_{s_c} \left(p_c \frac{\partial \varphi_c^m}{\partial n} - \varphi_c^m \frac{\partial p_c}{\partial n}\right) dS_c, \tag{13}$$

where $k_m = \omega_m / c_0$, with ω_m being the angular eigenfrequencies of the cavity; $N_c^m = \int_{V_c} \varphi_c^m \varphi_c^m dV_c$, c_0 is the speed of sound in air.

There exist various techniques for solving the above equation with different approximations.[19] A commonly used one is to assume that the eigenfunctions can be expressed as a series of rigid-walled acoustic modes

$$\varphi_c^m = \cos\left(\frac{m_x \pi}{L_x^c} x\right) \cos\left(\frac{m_y \pi}{L_y^c} y\right) \cos\left(\frac{m_z \pi}{L_z^c} z\right), \quad m_x, m_y, m_z = 0, 1, 2, \ldots, \tag{14}$$

where m_x, m_y, m_z are the modal indices in the x, y, z directions, and L_x^c, L_y^c, L_z^c are the cavity dimensions, respectively.

If a vibrating surface defined by S_v presents along the cavity boundary, the momentum equation is given by

$$\frac{\partial p_c}{\partial n} = -j\rho_0 \omega U, \tag{15}$$

where ρ_0 is the air density, and U is the boundary vibrating velocity. Similarly, an absorbing boundary S_α with its characteristic impedance being specified as Z_α can be described as (Neumann condition)[20]

$$\frac{\partial p_c}{\partial n} = -j\rho_0 \omega \frac{p_c}{Z_\alpha}. \tag{16}$$

Using the cavity mode shape functions in Eq. (14), the right-hand side term of Eq. (13) in the presence of a vibrating boundary S_v and an absorbing boundary S_α becomes

$$\int_{s_c} \left(p_c \frac{\partial \varphi_c^m}{\partial n} - \varphi_c^m \frac{\partial p_c}{\partial n}\right) dS_c = \int_{s_v} (j\rho_0 \omega U) \varphi_c^m dS_v + \int_{s_\alpha} \left(j\rho_0 \omega \frac{a_c^m}{Z_\alpha}\right) \varphi_c^m \varphi_c^m dS_\alpha. \tag{17}$$

Consider now the pressure field inside the cavity excited by a particular vibrating patch q on the cavity boundary.

Assuming that a sufficient number of patches have been defined at interfaces 1 and 2, the individual effect of the patch with a surface S_q and a vibrating velocity U_q can be described as

$$a_c^m\left[N_c^m(k^2-k_m^2)-j\rho_0\omega\int_{S_\alpha}(\varphi_c^m)^2dS_\alpha/Z_\alpha\right] = \int_{s_q}(j\rho_0\omega U_q)\varphi_c^m dS_q. \tag{18}$$

Note that subscript q for the exciting patch covers all the patches discretized along the cavity boundary. Then, by defining the acoustic impedance as the transfer function between the force and velocity, exerted onto a receiving patch p from an exciting patch q, respectively, one has[17]

$$Z_{pq}^c=\frac{F_p}{U_q}=\frac{\int_{s_p}p_c dS_p}{U_q}=\frac{\int_{s_p}\left(\sum_m a_c^m\varphi_c^m\right)dS_p}{U_q}. \tag{19}$$

Inserting Eq. (18) into Eq. (19) gives

$$Z_{pq}^c=\sum_m\frac{j\rho_0\omega}{N_c^m\left(k^2-k_m^2\right)-j\rho_0\omega\int_{S_\alpha}(\varphi_c^m)^2dS_\alpha/Z_\alpha}\times\int_{s_p}\varphi_c^m dS_p\int_{s_q}\varphi_c^m dS_q. \tag{20}$$

Equation (20) indicates that the impedance expression is a function of the cavity parameters (N_c^m, k_m, φ_c^r, Z_α, S_α) as well as the local properties at the exciting and receiving patch ($\int_{s_q}\varphi_c^m dS_q$ and $\int_{s_p}\varphi_c^m dS_p$). Using the modal expansion approach, relevant studies have addressed the detailed implementation procedure for a rigid rectangular cavity,[21] and a general cavity with arbitrary shape and general boundary conditions.[19] The calculated impedances between all the patches defined on interfaces 1 and 2 are then gathered in matrices $\mathbf{Z}_{11}^c$ and $\mathbf{Z}_{22}^c$ for the local description of the interface, and in matrices $\mathbf{Z}_{12}^c$ and $\mathbf{Z}_{21}^c$ for describing their mutual interactions.

An alternative way to determine these impedance matrices is to use other deterministic models such as FEM. This can be implemented by calculating the ratio between the averaged responses at a set of receiving patches, due to the excitation at one particular patch. This gives one column in the impedance matrix, like so,

$$\mathbf{Z}_{\mathrm{N1}}=\{\mathrm{Z}_{11};\mathrm{Z}_{21};\ldots;\mathrm{Z}_{\mathrm{N1}}\}. \tag{21}$$

This procedure is then repeated by replacing the excitation patch by N times to fill in all the elements for $\mathbf{Z}_{\mathrm{NN}}$, such that $\mathbf{Z}_{\mathrm{NN}}=[\mathbf{Z}_{\mathrm{N1}},\mathbf{Z}_{\mathrm{N2}},\ldots,\mathbf{Z}_{\mathrm{NN}}]$.

For a rigid rectangular cavity whose eigenfunction is analytically known in Eq. (14), a simple check has been conducted to compare the patch impedances obtained via using Eq. (20) and from FEM. Their numerical outputs are basically identical, which confirms the equivalence of using both methods to characterize the subsystem property. Nevertheless, the use of FEM is considered to be more applicable to real window designs with complex geometries. But the required n-DOF is also significantly increased compared with the modal based solution as a major drawback.

In order to predict the ensemble response of the system as shown in Fig. 3, the coupled equations for describing the interactions between the two interfaces can be written as

$$\begin{aligned}\mathbf{Y}_1(\mathbf{F}_1+\mathbf{Z}_1^r\mathbf{U}_1+\mathbf{Z}_{11}^c\mathbf{U}_1+\mathbf{Z}_{12}^c\mathbf{U}_2)&=\mathbf{U}_1,\\ \mathbf{Y}_2(\mathbf{Z}_{21}^c\mathbf{U}_1+\mathbf{Z}_{22}^c\mathbf{U}_2+\mathbf{Z}_2^r\mathbf{U}_2)&=\mathbf{U}_2,\end{aligned} \tag{22}$$

where $\mathbf{Y}_1$ and $\mathbf{Y}_2$ are the mobilities of the two interfaces as depicted in Eq. (10); $\mathbf{Z}_1^r$ and $\mathbf{Z}_2^r$ are the radiation impedances of the inlet and outlet acoustic domains, which can be of various types. $\mathbf{F}_1$ is the excitation force being applied to the inlet, and $\mathbf{U}_1$ and $\mathbf{U}_2$ are the vibrational responses of the two interfaces, respectively.

Once the velocity vectors from the coupled equations in Eq. (22) are solved, the silencing performance of the ventilation duct can be evaluated by calculating its sound transmission loss (TL). Here, two different TL definitions are suggested as

$$\begin{aligned}\mathrm{TL}_1&=10\log_{10}(\Pi_1^a/\Pi_2^a),\\ \mathrm{TL}_2&=10\log_{10}(\Pi_1^{a+s}/\Pi_2^a),\end{aligned} \tag{23}$$

where $\Pi_1^a=|p_0|^2S_1^a/(2\rho_0c_0)$ is the input sound power at the inlet aperture, if normal plane waves with a pressure amplitude p_0 is applied. $\Pi_2^a=\int_{S_2^a}\frac{1}{2}(p_2\times U_2^*)dS_2^a$ is the transmitted sound power from the outlet aperture toward the downstream, where p_2 is the averaged radiation patch pressure and U_2^* is the complex conjugate of the averaged patch velocity. S_1^a and S_2^a are the surface areas of the inlet and outlet apertures, respectively. The difference between TL_1 and TL_2 simply consists in whether the incident power is calculated with reference to the inlet aperture only, or the compound surface inclusive of the structural part (total area of interface 1, S_1^{a+s}). Given a normal plane wave incidence with a constant amplitude, TL_1 can be converted into TL_2 using a simple formula, if the structural part is deemed as rigid[5]

$$\begin{aligned}\mathrm{TL}_2&=10\log_{10}\left(\frac{S_a+S_s}{S_a}10^{\mathrm{TL}_1/10}\right)\\ &=\mathrm{TL}_1+10\log_{10}\left(\frac{S_a+S_s}{S_a}\right),\end{aligned} \tag{24}$$

where S_a and S_s are the surface areas occupied by the aperture and structure, respectively. Therefore, in the following numerical examples, only TL_1 is presented without any special notice.

III. NUMERICAL EXAMPLES

A. Empty ventilation duct

Consider the two-dimensional ducted ventilation system as shown in Fig. 2. Sections III A–III D present numerical studies for evaluating its acoustic performance using the proposed sub-structuring approach. As sketched in Fig. 4, the

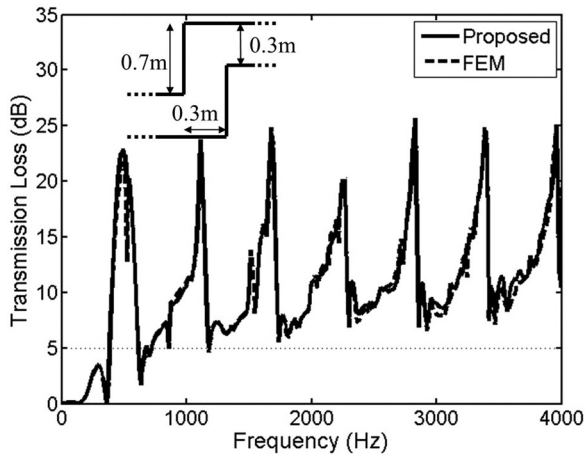

FIG. 4. Comparison of the TL results from the proposed approach and FEM for an empty ventilation duct. The system dimension is as sketched.

dimension of the ventilation duct is chosen as $H_1 = 0.7$ m, $H_2 = 0.3$ m, and $W = 0.3$ m, where two semi-infinite waveguides are connected as the inlet and outlet acoustic domains. The sound incidence to the inlet aperture is assumed as a normal plane wave with constant pressure amplitude across the frequency range. In such case, the sound energy is directed into and out of the duct without any loss elsewhere. Here, the expressions of $\mathbf{Z}_1^r$ and $\mathbf{Z}_2^r$ in Eq. (22), corresponding to semi-infinite ducts, are derived analytically based on the modal expansion approach as given in earlier publications.[17,22]

For this empty ventilation duct with rigid internal surfaces, validation is first carried out by comparing the system TL predicted using the proposed approach with that of a FEM simulation. This also benchmarks the silencing performance of the empty duct. In order to reach a frequency range up to 4000 Hz, the patch size defined over the coupling interface is required to be smaller than $\Delta_{\text{patch}} = \lambda_s/2 = 340/(2 \times 4000) \approx 0.04$ m. Therefore, both interfaces 1 and 2 in Fig. 3 (total height = 1 m) are segmented into 30 patches, with 9 patches over the aperture and 21 patches on the structure. The structural part is assumed as rigid here with a null mobility.

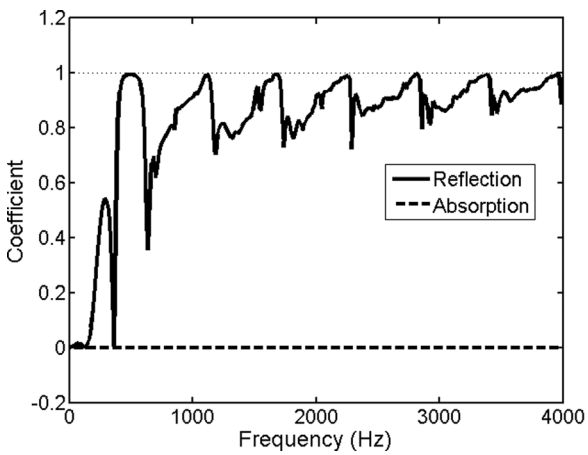

FIG. 5. Reflection coefficient R and absorption coefficient α of the empty ventilation duct.

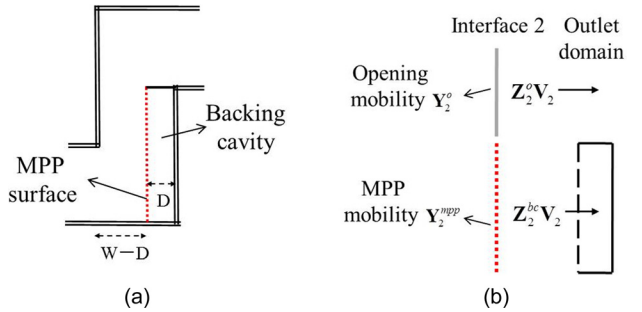

FIG. 6. (Color online) (a) Ventilation duct with integral MPP absorber for providing internal sound absorption. (b) Modified vibroacoustic formulation at interface 2.

A FEM model using commercial software COMSOL is also built for validation, where the inlet is excited by a plane wave radiation and the outlet end has a perfectly matched layer.[23] The enclosed acoustic domain is discretized into 40 000 nodes with a tightened criterion of $\Delta_{\text{fem}} = \lambda_s/8 \approx 0.01$ m. In Fig. 4, the TL results of the empty bended duct predicted by using the proposed approach and FEM simulation are presented from 10 to 4000 Hz, with a frequency step-size of 15 Hz. The excellent agreement between the two curves can be clearly seen, which validates the prediction accuracy of the proposed approach. However, in terms of computational time, the FEM model took around 300 s (5 mins) to run a simulation while the proposed approach requires only 12 s for the same accuracy (both on a laptop with Intel i5 processor, 4 GB memory). The reason is that the proposed approach built on a modal basis greatly reduces the n-DOF compared to that of the FEM model with a nodal basis, which would become even more crucial if a three-dimensional or larger system size is to be analyzed. It is worth noting that such significant reduction also benefits from the simple subsystem geometry (rectangular cavity and duct cross-sections), as formulated in Sec. II. For complex geometries requiring the use of FEM to obtain the subsystem characteristics, the calculation efficiency will be compromised to a certain degree.

It is also seen from Fig. 4 that, although the TL peaks of the empty duct can reach up to 25 dB at some particular frequencies, the averaged sound attenuation is still rather low. The TL lower-bound is typically capped at 5 dB across the frequency range, with a strong resonant pattern being observed. By separating the sound power being reflected back to the inlet and that being absorbed inside the ventilation duct, the system reflection coefficient R and absorption coefficient α can be calculated as[24]

$$R = \Pi_1^r/\Pi_1^a = (\Pi_1^a - \Pi_1^t)/\Pi_1^a, \qquad \alpha = (\Pi_1^t - \Pi_2^a)/\Pi_1^a, \tag{25}$$

where Π_1^r and Π_1^t are the reflected and transmitted sound powers at the inlet aperture, respectively. As shown in Fig. 5, the empty duct exhibits only the reactive behavior for sound attenuation with zero absorption, which is as expected. Therefore, one possible solution for enhancing the sound attenuation is to consider the application of sound absorbing treatment inside the empty ventilation duct, in order to

compensate for the deficiencies at numerous frequencies observed in Fig. 4.

B. Effect of adding MPP absorber

Traditional sound absorbing materials such as fiberglass or mineral wool can be well described using Eq. (16) through the complex acoustic impedance Z_α. However, fibrous absorbing materials have the disadvantages of being flammable, bulky, non-durable, and unsafe for human health. Instead, a MPP absorber[25] provides a non-fibrous alternative, and its effectiveness is discussed here. Consider the ventilation duct with an integral MPP absorber as shown in Fig. 6(a). The MPP surface is placed directly facing the inlet aperture, forming a backing acoustic cavity of depth D with the rear wall. The duct width left for air passage is decreased from W to W - D accordingly.

Previous studies[17,24] have emphasized the importance of modeling MPP as an integral part of the vibroacoustic system, since its *in situ* sound absorption is strongly dependent on the surrounding environment. Comparing the system shown in Fig. 6(a) with the empty duct in Fig. 2, the coupling through the inlet interface remains unchanged. Therefore, only the modeling for interface 2 is considered in Fig. 6(b). For the modeling of the MPP surface, an equivalent mobility treatment has been developed, which averages the vibration of the panel frame and air-mass motion inside the micro-holes and gives[24]

$$\mathbf{Y}^{mpp} = (1-\sigma)\mathbf{Y}^{p} + \left(\frac{\sigma}{Z_h \Delta s}\right)\mathbf{I}, \tag{26}$$

where $\mathbf{Y}^p$ is the structural mobility of the panel; σ is the percentage of area occupied by the holes, or referred to as the perforation ratio; Δs is the surface area of the divided patch; $\mathbf{I}$ is an identity matrix of the same order as the number of patches; Z_h is the characteristic acoustic impedance of a single hole, with its resistance part Z_h^r and reactance part Z_h^i being expressed as

$$\begin{aligned} Z_h^r &= \frac{32\eta t}{d^2}\left[\left(1+\frac{k^2}{32}\right)^{1/2} + \frac{\sqrt{2}}{32}k\frac{d}{t}\right], \\ Z_h^i &= j\rho_0\omega t\left[1+\left(9+\frac{k^2}{2}\right)^{-1/2} + 0.85\frac{d}{t}\right], \end{aligned} \tag{27}$$

where η is the air viscosity, t is the MPP thickness, d is the hole diameter, and k is the perforation constant $k = d\sqrt{\rho_0\omega/4\eta}$. Note that Eq. (26) is generally applicable to both rigid and flexible MPPs.

Using the same compound interface treatment as in Eq. (10), the mobility of interface 2 can be determined by combining the aperture mobility and equivalent MPP mobility as

$$\mathbf{Y}_2 = \begin{bmatrix} \mathbf{Y}_2^o & \\ & \mathbf{Y}_2^{mpp} \end{bmatrix}. \tag{28}$$

As to the modeling of the radiation domain, this can be done by slightly changing $\mathbf{Z}_2^r$ in Eq. (22) to

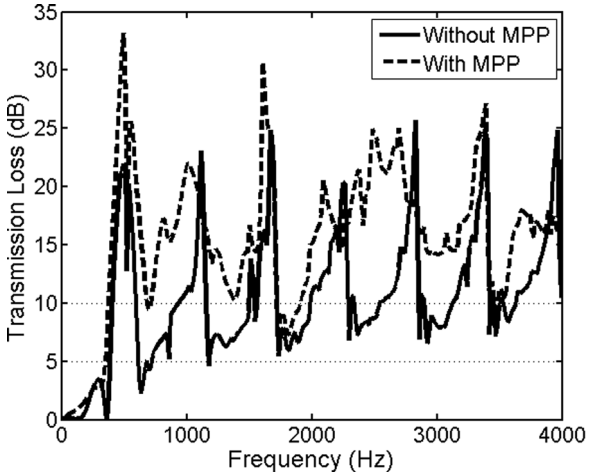

FIG. 7. Effect of the additional MPP absorber on TL.

$$\mathbf{Z}_2^r = \begin{bmatrix} \mathbf{Z}_2^o & \\ & \mathbf{Z}_2^{bc} \end{bmatrix}, \tag{29}$$

where $\mathbf{Z}_2^o$ is the radiation impedance at the upper opening of interface 2. Duct impedance is used here in the simulation examples. $\mathbf{Z}_2^{bc}$ is the impedance of the acoustic cavity backing the MPP. The same formulation as in Eq. (20) is applicable.

The sound absorption performance of the MPP absorber strongly depends on a set of parameters including the hole diameter d, panel thickness t, perforation ratio σ, backing cavity depth D, as well as the dimension and aperture size of the duct. In the simulation, the MPP parameters are first assumed as: $d = t = 0.2$ mm, $\sigma = 1\%$, $D = 0.1$ m, with the same duct dimension as in Fig. 4. In Fig. 7, the predicted TL of the system with the MPP absorber is compared with the benchmark TL of the empty duct. It can be seen that the added MPP absorber significantly enhances the sound attenuation of the empty duct, resulting in an averaged 5 dB increase across the frequency range and a 10 dB increase in some particular frequencies. This clearly demonstrates the potential of using MPP to achieve a better sound insulation.

In order to quantify the actual sound absorption provided by the MPP absorber, the reflection and absorption coefficients of the system are calculated and plotted in Fig. 8. It can be observed that the sound absorption is prominent and becomes the dominant mechanism for sound attenuation, while the reflection effect seems to provide compensations at the absorption valleys. To explain this, the sound waves entering into the duct through the inlet aperture first interact with the MPP absorber before the reactive effect takes place. At the absorber's effective frequencies, the sound energy is efficiently damped by the distributed tiny holes and radiation back to the main duct is reduced, as evidenced by the low value in the reflection coefficient R. When the MPP absorption is less efficient due to resonances of the backing cavity (α valleys), the bended duct as a reactive device still enables strong sound reflection as explained in Fig. 5. Such a hybrid sound attenuation mechanism ultimately maintains the system TL at a relatively high level as seen from Fig. 7.

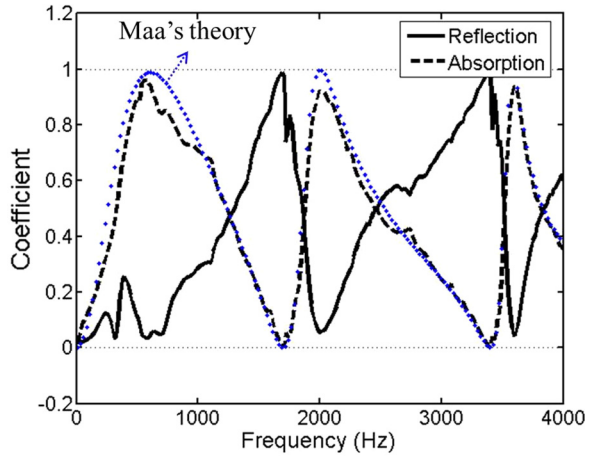

FIG. 8. (Color online) Reflection coefficient R and absorption coefficient α of the ventilation duct with a MPP absorber. The dotted line plots he Maa's theory for a MPP absorber in impedance tube setting.

It is also interesting to note that the actual sound absorption curve of the MPP closely resembles the theoretical curve when it is placed in an impedance tube for testing (known as Maa's theory[25]). This observation also supports the above discussion and indicates that the absorption mechanism is primary and dominating. Based on this, one may suggest that a better absorption design can be achieved by selecting the right MPP absorber with optimized parameters. But still, the overall silencing performance is determined by the hybrid effects of sound reflection and absorption. Aiming an optimal TL response, one may need to balance these two effects for a desired broadband performance in the design frequency of interest.

C. Parametric studies

Following the previous mechanism investigations, a numerical study for analyzing the possible influence of system parameters is presented. It is assumed that the basic system configuration in Fig. 6 remains unchanged for all the simulated cases, whereas the parameters associated with the MPP absorber can vary within a certain range. In order to alter the impedance of the MPP surface, the hole diameter d and its

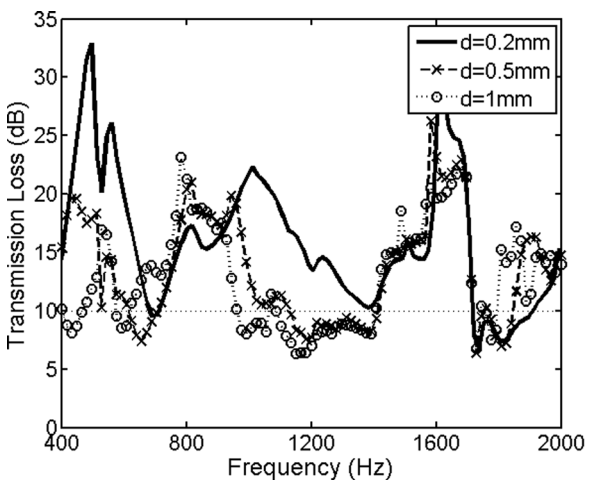

FIG. 9. TL variations with varying MPP hole diameter d.

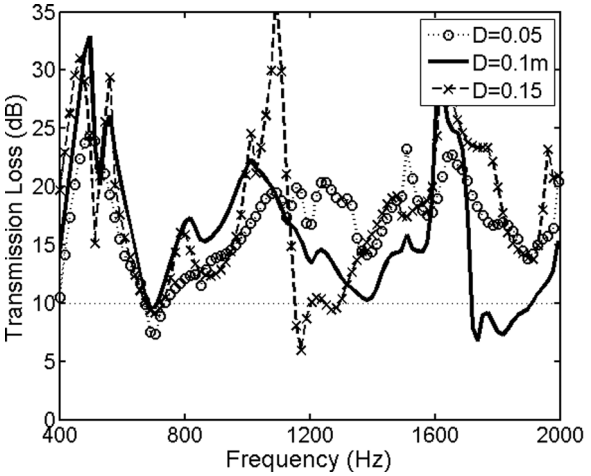

FIG. 10. TL variations with varying backing cavity depth D of the MPP.

influence are first considered. In Fig. 9, the TL responses corresponding to three MPP cases with the hole diameter d varying from 0.2 to 1 mm are compared. The MPP thickness t is simply assumed as equal to d, and other parameters are fixed as: $\sigma = 1\%$, $D = 0.1$ m. It can be seen that a smaller hole diameter generally leads to a better silencing performance in a medium frequency range from 400 to 2000 Hz. Its correlation with the absorption coefficient curve α has been checked, which confirms that the improvement is mainly attributed to an enhanced and widened absorption band provided by the MPP with smaller holes. It is then suggested that an efficient sound absorption would call for a small hole size d (the panel thickness t needs to be matched), in agreement with similar observations reported in some other studies.[24–26] However, it is worth mentioning that this argument is not universally true and requires other factors such as backing cavity size and intended frequency range to be considered simultaneously. Beside the hole diameter, similar analyses on the panel thickness and perforation ratio have also been performed (not shown here). The major conclusion from these analyses is that the system TL response is very sensitive to the variation of MPP parameters.

By fixing the perforation parameters as $d = t = 0.2$ mm, $\sigma = 1\%$, which gives the best broadband performance in Fig. 9, the influence of backing cavity size of the MPP is investigated by comparing three cases with $D = 0.05$, 0.1, and 0.15 m, respectively. As shown in Fig. 10, the variation of the TL curves across the frequency range of interest is clearly observed. But unlike the previous discussion on the hole diameter, no general variation trend can be concluded from the comparison in Fig. 10. The reason is that different cavity depths not only affect the absorption curve α by altering the resonant behavior of the absorber, but also changes the reflection curve R due to the fully coupled nature of the acoustic fields.

From the above analyses, it can be seen that the parameter changes provide considerable scope for the tuning of system TL, whilst the proposed sub-structuring approach offers a computationally tractable tool. Before starting the optimization study, some interim conclusions rising from the present analyses can be summarized:

(1) In order to achieve a better sound attenuation, controlling the MPP perforation parameters seems to be more important than varying the backing cavity size. The former determines the absorption ability and bandwidth by changing the surface impedance, while the latter only alters the resonant behavior of the coupled acoustic fields.
(2) Generally, a smaller hole diameter d can offer a more effective sound dissipation and a broader absorption bandwidth. An appropriate panel thickness t and perforation ratio σ also needs to be matched with the selection of d.
(3) The influences of the involved parameters are interconnected. In order to seek the best result, one needs to perform system optimization with multiple variables.
(4) A balance between the sound reflection and absorption effect is needed for achieving an overall broadband TL performance.

D. Optimization study

The proposed sub-structuring model significantly reduces the computational cost compared with FEM and is employed to perform the system optimization. By assuming a fixed duct dimension and aperture size as in Fig. 4, the parameters associated with the MPP absorber $\{t, d, \sigma, \mathrm{D}\}$ are to be optimized for a given frequency range of interest. The objective function is defined as to minimize the total sound power transmitted from the outlet aperture, which integrates the value of Π_2^a at all the discrete frequency points.[27] This enables us to identify the best combination of parameters which gives the best broadband TL performance. Being mindful of the validity of Eq. (27), the hole diameter d (as well as panel thickness t) is varied from 0.2 to 1 mm. The perforation ratio σ is constrained within 0.3% to 2%, and the backing cavity depth D can vary from 0.02 to 0.15 m. Note that the flow rate consideration is temporarily neglected, which can be integrated into the optimization model for a more practical analysis.

The first optimization study (referred to as Opt 1) considers d and D as variables, where the perforation ratio σ is fixed at 1%. The targeted frequency from 400 to 2000 Hz is linearly divided into 110 frequency points for the integration of the total power Π. The d interval (0.2–1 mm) is divided into 17 points with an increment of 0.05 mm, and the D interval (0.02–0.15) m is divided into 27 points with an increment of 0.005 m. This results in 459 combinations for the exhaustive search of the optimal TL. Using the proposed approach, the calculation time required for each case is roughly 9 s. The total time for the optimization is therefore $459 \times 9 \approx 4000$ s (about 1 h).

In Fig. 11, the distribution of the calculated total power as a function of the two variables d and D is presented, which demonstrates the existence of the minima at $d = t = 0.2$ mm, $D = 0.06$ m (total power $\Pi = 0.0037$ w). By looking at a particular value of D while gradually decreasing the hole diameter d, the general trend of an increased sound attenuation performance is observed. However, by fixing d at a certain value while varying the cavity depth D does not show any generalized and conclusive behavior. Both observations are in consistent with the observations made in Sec. III C.

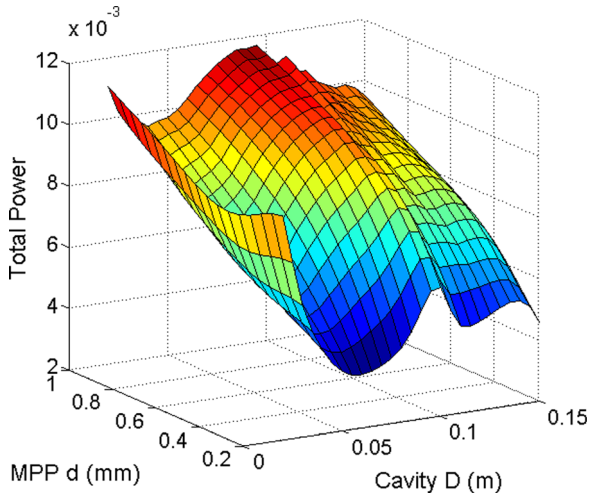

FIG. 11. (Color online) Total power vs MPP hole diameter d and backing cavity depth D, for the first optimization case study (Opt 1).

Then, consider a second optimization study (Opt 2) with the inclusion of an additional variable, perforation ratio σ. The frequency and D intervals are the same as Opt 1, whereas the d interval is narrowed to (0.2–0.5) mm with 7 points. The σ interval (0.3%–2%) is evenly divided into 18 points with an increment of 0.1%. This results in a total number of $7 \times 27 \times 18 \approx 3400$ cases, and the total computational time is extended to 8.5 h. The minima of the total sound power from Opt 2 is located at $d = t = 0.2$ mm, $D = 0.05$ m, $\sigma = 0.5\%$, and the total power Π of this combination is further decreased to 0.0029 w, compared with 0.0037 w in Opt 1. This leads to an average 1 dB improvement in the overall sound reduction curve.

In Fig. 12, the TL curves corresponding to the optimal results from Opt 1 and 2 are presented. Both curves are seen to exhibit broadband attenuation performance in the targeted frequency range, with an averaged TL of about 15 dB. The little improvement in the TL response from Opt 2 can be also identified by looking at the TL lower-bound. Further

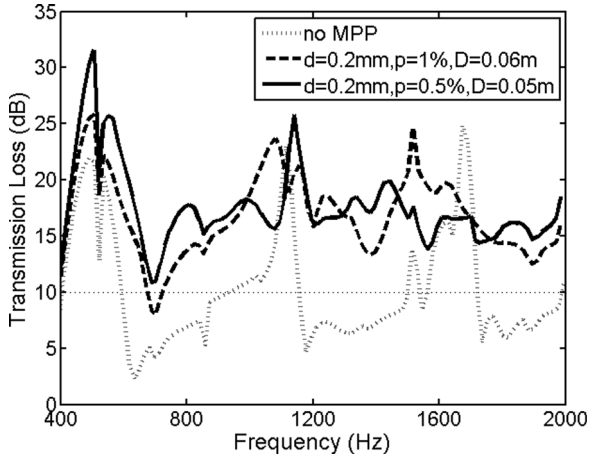

FIG. 12. Optimized TLs from the two optimization case studies.

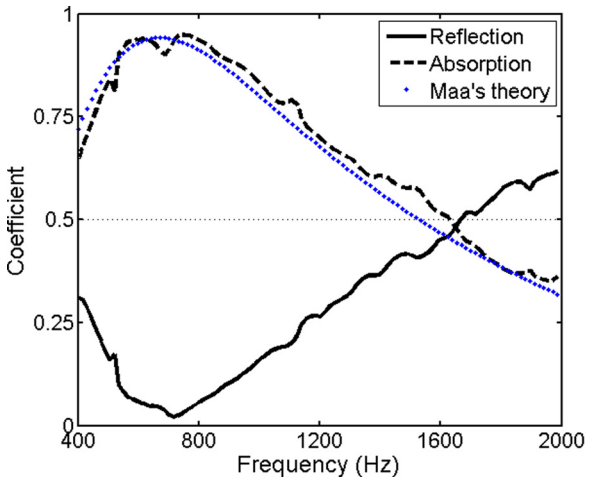

FIG. 13. (Color online) Reflection coefficient R and absorption coefficient α of the system with the optimized parameters from the second optimization study (Opt 2).

analysis on the reflection and absorption coefficients provides insight to the optimized results. In Fig. 13, the R and α curves corresponding to the optimized result from Opt 2 are plotted. Below 1600 Hz, the sound absorption provided by the MPP absorber is more effective than the sound reflection provided by the bended duct. After the α maximum at 800 Hz, the gradual decrease in the absorption curve is compensated by an increase in the reflection curve. The two curves intersect at around 1600 Hz, where $R = \alpha = 0.5$. This eventually shows the well-balanced behavior of the hybrid effects in the optimized configuration.

IV. CONCLUSIONS

A sub-structuring approach to model the complex structural-acoustic coupling involved in ducted ventilation systems has been proposed. The system ensemble is decoupled into a set of subsystems, allowing the characterization of their transfer functions at the separation interfaces. The assembling treatment is performed by using a patch based interface matching technique. For a representative ventilation duct with regular geometry, a numerical model has been built to predict its sound attenuation performance. The involved subsystems were modeled analytically using modal based solutions. By comparing the simulation results with a FEM model, the convergence and prediction accuracy of the proposed model have been validated.

Through the presented numerical examples, the potential of using a MPP absorber to improve the sound attenuation performance of an empty ventilation duct has been shown. With MPP, the system exhibits a hybrid sound attenuation mechanism with combined reactive and dissipative effects. The sound absorption provided by the MPP absorber basically dominates the overall attenuation, and the absorption valleys due to the backing cavity resonances are compensated by the sound reflection provided by the bended duct.

The sensitivity of the system response to parameter changes has been shown. In particular, the effects of varying MPP hole diameter d and backing cavity depth D were discussed. These two parameters are effective in controlling the MPP surface impedance and the resonant frequencies of the system. Using the proposed approach, two optimization studies were conducted to search for the optimal combination of parameters. The optimized results exhibited broadband attenuation performance through well-balancing of the sound reflection and absorption effects. The flow rate analysis can be further included to guide a more comprehensive design and optimization for the present device.

As a general comment on the merits of the proposed approach, the associated computational cost was shown to be significantly lower compared with FEM. Plus with the modular nature of the approach, optimization studies were able to be carried out efficiently. Meanwhile, the proposed sub-structuring modeling framework enables the construction of hybrid numerical models, where the subsystem properties can be obtained using different numerical methods. Benefiting from a patch based interface treatment, system assembly at the connecting boundaries can be performed in a very convenient and flexible way. This could further extend the applicability of the proposed approach to tackle more challenging engineering applications involving subsystems with complicated geometries or different orders of n-DOF, for fulfilling the real design need of such systems.

ACKNOWLEDGMENT

This material is based on research/work supported by the Singapore Ministry of National Development and National Research Foundation under L2 NIC Award No. L2NICCFP1-2013-9. The authors also wish to acknowledge two grants from the Research Grants Council of Hong Kong Special Administrative Region, China (Grant Nos. PolyU 5103/13E and PolyU 152026/14E).

[1]D. Etheridge and M. Sandberg, *Building Ventilation: Theory and Measurement* (John Wiley & Sons, Chichester, UK, 1996), 754 pp.
[2]D. J. Oldham, M. H. De Salis, and S. Sharples, "Reducing the ingress of urban noise through natural ventilation openings," Indoor Air **14**, 118–126 (2004).
[3]E. B. Viveiros, B. M. Gibbs, and S. N. Y. Gerges, "Measurement of sound insulation of acoustic louvres by an impulse method," Appl. Acoust. **63**, 1301–1313 (2002).
[4]C. D. Field and F. R. Fricke, "Theory and applications of quarter-wave resonators: A prelude to their use for attenuating noise entering buildings through ventilation openings," Appl. Acoust. **53**, 117–132 (1998).
[5]M. H. F. De Salis, D. J. Oldham, and S. Sharples, "Noise control strategies for naturally ventilated buildings," Build. Environ. **37**, 471–484 (2002).
[6]J. Kang and M. W. Brocklesby, "Feasibility of applying micro-perforated absorbers in acoustic window systems," Appl. Acoust. **66**, 669–689 (2005).
[7]J. Kang and Z. Li, "Numerical simulation of an acoustic window system using finite element method," Acta Acust. Acust. **93**, 152–163 (2007).
[8]H. Huang, X. Qiu, and J. Kang, "Active noise attenuation in ventilation windows," J. Acoust. Soc. Am. **130**, 176–188 (2011).
[9]Z. H. Wang, C. K. Hui, and C. F. Ng, "The acoustic performance of ventilated window with quarter-wave resonators and membrane absorber," Appl. Acoust. **78**, 1–6 (2014).
[10]J. Rohlfing and P. Gardonio, "Ventilation duct with concurrent acoustic feed-forward and decentralised structural feedback active control," J. Sound Vib. **333**, 630–645 (2014).
[11]R. H. Lyon, R. G. DeJong, and M. Heckl, "Theory and application of statistical energy analysis, second edition," J. Acoust. Soc. Am. **98**, 3021–3021 (1995).

[12]M. Ouisse, L. Maxit, C. Cacciolati, and J.-L. Guyader, "Patch transfer functions as a tool to couple linear acoustic problems," J. Vib. Acoust. **127**, 458–466 (2004).
[13]R. Kirby, "Modeling sound propagation in acoustic waveguides using a hybrid numerical method," J. Acoust. Soc. Am. **124**, 1930–1940 (2008).
[14]J. Poblet-Puig and A. Rodríguez-Ferran, "Modal-based prediction of sound transmission through slits and openings between rooms," J. Sound Vib. **332**, 1265–1287 (2013).
[15]R. S. Langley and J. A. Cordioli, "Hybrid deterministic-statistical analysis of vibro-acoustic systems with domain couplings on statistical components," J. Sound Vib. **321**, 893–912 (2009).
[16]C. Díaz-Cereceda, J. Poblet-Puig, and A. Rodríguez-Ferran, "The finite layer method for modelling the sound transmission through double walls," J. Sound Vib. **331**, 4884–4900 (2012).
[17]X. Yu, L. Cheng, and J.-L. Guyader, "Modeling vibroacoustic systems involving cascade open cavities and micro-perforated panels," J. Acoust. Soc. Am. **136**, 659–670 (2014).
[18]X. Yu, L. Cheng, and J.-L. Guyader, "On the modeling of sound transmission through a mixed separation of flexible structure with an aperture," J. Acoust. Soc. Am. **135**, 2785–2796 (2014).
[19]N. Totaro, S. Forget, and J.-L. Guyader, "iPTF methods: How Green's identity and FEM solver can be used for acoustic inverse methods," in *Proceeding of EuroNoise* (2015), pp. 903–908.
[20]W. Kropp and J. Bérillon, "A theoretical model to consider the influence of absorbing surfaces inside the cavity of balconies," Acta Acust. Acust. **86**, 485–494 (2000).
[21]J.-D. Chazot and J.-L. Guyader, "Prediction of transmission loss of double panels with a patch-mobility method," J. Acoust. Soc. Am. **121**, 267–278 (2007).
[22]X. Yu and L. Cheng, "Duct noise attenuation using reactive silencer with various internal configurations," J. Sound Vib. **335**, 229–244 (2015).
[23]A. Comsol, *COMSOL Multiphysics User's Guide*, September (2005).
[24]X. Yu, L. Cheng, and X. You, "Hybrid silencers with micro-perforated panels and internal partitions," J. Acoust. Soc. Am. **137**, 951–962 (2015).
[25]D.-Y. Maa, "Potential of microperforated panel absorber," J. Acoust. Soc. Am. **104**, 2861–2866 (1998).
[26]D. Y. Maa, "Practical single MPP absorber," Int. J. Acoust. Vib. **12**, 3–6 (2007).
[27]X. Yu, Y. Tong, J. Pan, and L. Cheng, "Sub-chamber optimization for silencer design," J. Sound Vib. **351**, 57–67 (2015).